Damping dispersion of excitonic polaritons in CdS

Karl-Heinz Pantke and Immanuel Broser

Institut für Festkörperphysik der Technischen Universität Berlin,
Hardenbergstrasse 36, D-1000 Berlin 12, Germany

(Received 1 June 1993)

We extract the damping dispersion $\Gamma(\omega)$ of excitonic polaritons in CdS on the basis of precise measurements of the transmission and reflectance. On the low-energy side of the $A_{n=1}$ exciton, the damping, which corresponds to the inverse dipole dephasing time, is independent of temperature, due to the scattering with impurities. On the high-energy side the damping increases with temperature and with the detuning from the resonance frequency due to the scattering with acoustic-phonons between different polariton modes. The probability of exciton-phonon scattering mediated by the deformation potential and by the piezoelectric effect is calculated and the measured damping spectrum is described qualitatively and quantitatively. By analyzing our results different relaxation channels of acoustic-phonon scattering are clearly discriminated.

I. INTRODUCTION

The dispersion relations of excitonic polaritons in semiconductors, expressed by the dielectric function $\epsilon(\omega,k)$, contain a damping parameter Γ which describes the interaction with all other particles and quasiparticles such as impurities and phonons. Γ is commonly assumed to be a wave-vector-independent constant. It was pointed out in the theoretical work of Tait and Weiher[1] that the interaction of polaritons with acoustic phonons yields a wave-vector-dependent scattering probability and, consequently, a dispersion of the damping term $\Gamma(\omega)$.

A spectral dependence of the damping term $\Gamma(\omega)$ has been introduced by several authors to explain experimental results received in the frequency domain from Raman scattering,[2] Brillouin scattering,[3,4] and transmission experiments.[5-7] Yu and Shen[2] introduced a wave-vector-dependent damping for the 1-s yellow exciton in Cu_2O due to acoustic-phonon scattering to explain the dispersion in the experimental Raman cross sections. A significant broadening of the Brillouin peaks was observed by Ulbrich and Weisbuch[3] in GaAs and by Shigenari, Lu, and Cummins[4] in CdS during laser scanning from below to above the exciton resonance frequency. From transmission and reflection experiment a detuning dependence proportional to the group velocity of the polariton was reported by Broser, Pantke, and Rosenzweig[5] for the region just around the resonance frequency of the $A_{n=1}$ exciton in CdS. They speculated that the observed spectral dependence is due to the scattering by charged impurities, and neglected the role of acoustic phonons. Dagenais and Sharfin[6] fitted the measured transmission in the region between the $A_{n=1}$ and $B_{n=1}$ resonances in CdS assuming a scattering of polaritons by LA-acoustic phonons via the deformation-potential interaction, and obtained a reasonable agreement between experiment and theory. However, they completely ignored the contributions from other intrinsic scattering processes other than deformation-potential interactions. Similar results were received by Refs. 7 and 8.

The damping parameter Γ corresponds to the inverse exciton polariton dipole dephasing time T_2, and its dispersion can be also observed in the time domain.[9-11] The first experiments by means of time-resolved, nondegenerate four-wave mixing in CuCl were performed by Masumoto, Shionoya, and Takagahara.[9] The observed energy dependence of the dephasing times at about 100-kW peak power excitation was attributed to the process of polariton-polariton scattering under high excitation. The authors failed to measure the low-intensity dephasing time, and did not obtain information about intrinsic relaxation channels, such as scattering of polaritons by phonons. Very recently, Vallée, Bogani, and Flytzanis[10] measured the dephasing time of the exciton polariton in CuCl by use of a time-resolved coherent two-photon excitation and probe technique. They obtained dephasing times in the low-intensity regime; however, their technique restricted the measurements to discrete photon energies of the probe beam. From the dephasing times measured at two spectral positions, they concluded that for low temperatures the deformation-potential scattering and the piezoelectric scattering contribute to the relaxation process.

In the present paper we extract the damping spectrum of exciton polaritons from measurements in the frequency domain. Measurements in the frequency domain can be performed in the low-intensity regime and, furthermore, they are not limited by discrete values of the spectrum as in two-photon excitation. In contrast to other publications[6,7] our analysis is based on precise measurements of reflectance and transmission spectra in the region between the $A_{n=1}$ and $B_{n=1}$ exciton polariton, which establishes both the real and the imaginary parts of the dielectric function. The damping spectrum obtained will be described quantitatively, and different scattering processes discriminated.

II. EXPERIMENT

Measurements in the temperature range of 2–30 K were performed with crystals of about 1-mm^2 area and about 10-μm thickness. The CdS samples of good optical quality, as-grown in the vapor phase, were placed free from any mechanical stress between paper masks and were immersed in a variable-temperature helium cryo-
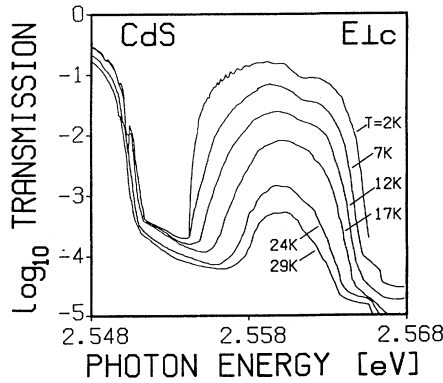
FIG. 1. Temperature-dependent transmission spectra of a 10-μm-thick CdS sample within the spectral range of the $A_{n=1}$ and $B_{n=1}$ exciton. The photon energies have been normalized to the 2-K spectrum.

stat. As a tunable and monochromatic light source we used a unit consisting of a xenon high-pressure lamp and a two-grating monochromator with a resolution of 0.25 Å at a slit width of 40 μm. The light passing the exit slit of the monochromator was polarized in $E \perp c$ and focused onto the sample. Depolarization effects inside the crystal required a second polarization filter $E \perp c$ behind the sample. To separate weak signals from stray light and luminescence the divergence of the transmitted beam was restricted by small pin holes and finally detected by a photomultiplier. All spectra wee recorded for a normal angle of incidence. With this apparatus a transmission of less than 10^{-5} could be detected.

From a number of investigated crystals we selected a 10- (sample No. 1) and a 10.25-μm- (sample No. 2) thick sample, which, however, showed different transmission spectra in the region of free and bound excitons.

The predominant structures of the measured transmission spectra of sample No. 1 in Fig. 1 are due to the absorption of the free $A_{n=1}$ exciton and the free $B_{n=1}$ exciton, which is partly cutoff on the high-energy edge of the figure. The sharp line on the low-energy side of the $A_{n=1}$ exciton corresponds to the creation of an impurity-bound exciton complex. While, with increasing temperature, the transmission of the low-energy wing of the $A_{n=1}$ ex-
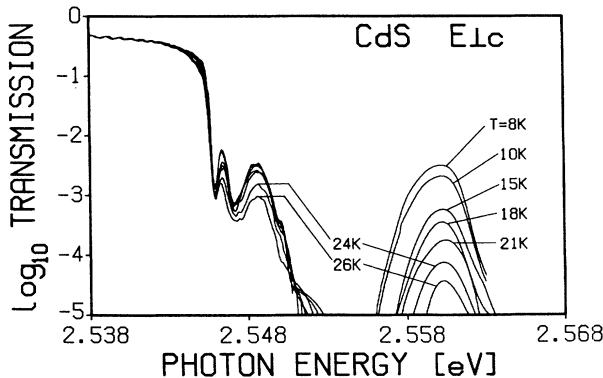

FIG. 2. Temperature-dependent transmission spectra of a 10.25-μm-thick CdS sample within the spectral range of the $A_{n=1}$ and $B_{n=1}$ exciton. The photon energies have been normalized to the 8-K spectrum.
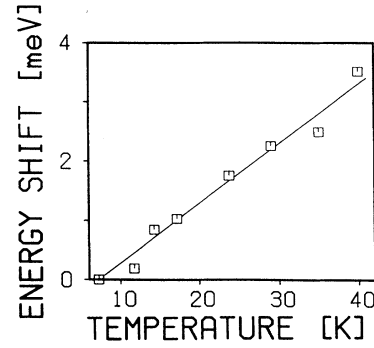

FIG. 3. Temperature-dependent energy shift of exciton lines.

citon is nearly constant, a drastic decrease of intensity in the window of transparency between the free exciton resonances is observed. The photon energies have been normalized to the 2-K spectrum to compensate for the temperature dependence of the band-gap energy, which has been determined from the shift of impurity-bound exciton lines.

The transmission spectra of the 10.25-μm-thick sample No. 2 in Fig. 2 reveal as well a pronounced decrease of intensity with temperature in the window of transparency between the free exciton resonances, while on the low-energy side of $A_{n=1}$ the transmission is independent of temperature. However, in comparison with sample No. 1 the free and bound exciton lines are broadened and the overall transmission is much weaker.

The measured shift of exciton lines with temperature in Fig. 3 can be fitted by a linear dependence. We obtain $\Delta E_{\exp} = -0.10$ meV/K, which is a little larger than the value of the band-gap shift $\Delta E_{the} = -0.079$ meV/K calculated by Bleil[12] and Azuma[13] considering the interaction of electrons and acoustic phonons via the deformation potential and the piezoelectric potential and the thermal expansion of the lattice.

Measured reflectance and transmission spectra of sample No. 1 are compared in Fig. 4 for $T = 8$ and 29 K. For low temperatures the minimum of reflection of the $A_{n=1}$ exciton coincides with the minimum of transmission near the resonance frequency of the longitudinal exciton ω_L. Up to 29 K, the shape of the reflectance changes only slightly with increasing temperature, while the transmission decreases as described above. With increasing temperature the reflectance increases slightly near the longitudinal frequency ω_L of the $A_{n=1}$ exciton and decreases slightly at the resonance frequency ω_0 of the $B_{n=1}$ exciton, which shows a double structure, due to the k-linear term.[14]

In the following sections we analyze the measured spectra in detail to elaborate the damping dispersion of excitonic polaritons and, furthermore, to fit the curve obtained.

III. THE DAMPING SPECTRUM $\Gamma(\omega)$ OF EXCITONIC POLARITONS

The optical spectra in the region of the $A_{n=1}$ and $B_{n=1}$ excitons can be calculated from the dielectric function $\epsilon(\omega,k) = (n^*)^2 = c^2 k^2 / \omega^2(k)$, given by the following expression:[15]

$$\epsilon(\omega,k)=\epsilon_0\left[1+\frac{2\omega_{0_{An=1}}\omega_{LT_{An=1}}}{\omega_{0_{An=1}}^2-\omega^2+\dfrac{\hbar k^2}{M_A}\omega_{0_{An=1}}-i\Gamma(k)\omega}+\frac{2\omega_{0_{Bn=1}}\omega_{LT_{Bn=1}}}{\omega_{0_{Bn=1}}^2-\omega^2+\dfrac{\hbar k^2}{M_B}\omega_{0_{Bn=1}}\pm\phi k-i\Gamma(k)\omega}\right] \tag{1}$$

where ϵ_0 is the background dielectric constant, ϕk the k-linear term, and $\omega_{0A,Bn=1}$, $\omega_{LTA,Bn=1}$, $M_{A,B}$ are the resonance frequencies, longitudinal-transverse splittings, and the effective masses of the $A_{n=1}$ and $B_{n=1}$ excitons, respectively. The damping parameter $\Gamma(k)$ describes the dissipation of excitonic polaritons and is related to the exciton polariton dipole dephasing time $T_2(k)$ by $\Gamma(k)=2/T_2(k)$.

Equation (1) can be derived from the dielectric function of Lorentzian oscillators, in which the resonance frequencies are replaced by k-dependent exciton energies. The so-called "spatial dispersion" leads to the existence of more than one propagation mode for one frequency, and additional boundary conditions (ABC's) are necessary to distribute the incoming field strength on the different modes. Furthermore, spatial dispersion of the medium leads to a significant k dependence of the damping parameter $\Gamma(k)$, because scattering processes between different branches due to acoustic phonons are possible.

The line shape of the optical spectra depend on all pa-

rameters of the dielectric function including the damping parameter $\Gamma(k)$. However, surface experiments such as reflectance are mainly governed by the real part of the dielectric function and depend only weakly on the temperature (see Fig. 4), while the absorption is more influenced by the imaginary part which is incorporated into the damping parameter $\Gamma(k)$. In order to elaborate the damping parameter $\Gamma(k)$, we first establish the real part of the dispersion for line-shape fits of the measured reflectance. In these fits we used Pekar's ABC[16] and neglected the exciton-free surface layer,[17] the spatial dispersion ($M=\infty$), and the k-linear term of the $B_{n=1}$ exciton. The parameters of the real part of the dielectric function $\epsilon=(\omega,k)$ at $T=2$ K received from the analysis of the reflectance are summarized in Table I.

We restrict the analysis of the transmission spectra to the spectral range $\omega<\omega_{0Bn=1}$, and neglect the spatial dispersion of the B resonance. The amplitude of transmitted light through a plane parallel plate of thickness d is given by[18]

$$E_T=-E_0e^{-ik_0d}\frac{4(1+F)(n_1S_1+n_2S_2F)S_1S_2}{\{(1+F)-n_1T_1-n_2T_2F\}^2S_1^2S_2^2-4(n_1S_2+n_2S_1F)^2},$$

$$S_i=e^{ik_id}-e^{-ik_id},$$

$$T_i=S_i\frac{1}{e^{ik_id}+e^{-ik_id}},$$

$$F=-\frac{n_1^2-\epsilon_0}{n_2^2-\epsilon_0},$$

$$\tag{2}$$

where the complex refractive indices n_i and k vectors k_i are calculated from Eq. (1). To derive Eq. (2), Pekar's ABC has been assumed for the front and back surfaces. An exciton-free surface layer has been neglected at each
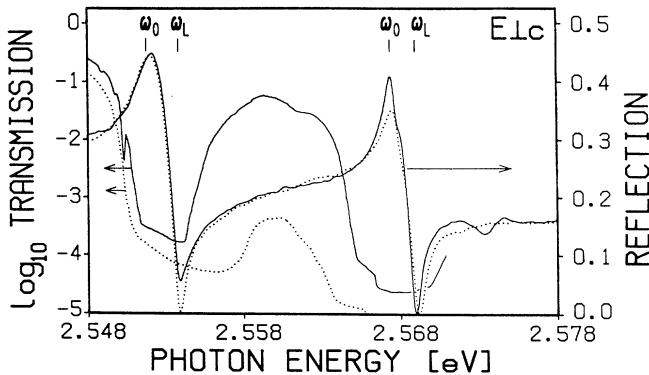
surface for simplicity, because its consideration would change the calculated transmission only by a few percent, in contrast to the variation of the measured intensity of about 4 orders of magnitude.

The two samples under investigation are nearly equal in thickness and the analysis of measured reflectance reveals more or less identical sets of parameters for the real part of the dielectric function. The damping dispersion $\Gamma(k)$ is the only free parameter to describe the measured transmission curves which, however, has to be different

FIG. 4. Reflection and transmission spectra of a 10-μm-thick CdS sample within the spectral range of the $A_{n=1}$ and $B_{n=1}$ exciton for $T=8$ K (solid curves) and $T=29$ K (dashed curves). The photon energies have been normalized to the 8-K spectra.

TABLE I. Parameters of the real part of the dielectric function $\epsilon=(\omega,k)$ determined from line-shape fits of the reflectance at $T=2$ K for sample Nos. 1 and 2.

$\omega_{0An=1}$	2.5518 eV
$\omega_{LTAn=1}$	2.0 meV
$M_{A\perp}$	$0.9m_0$
$\omega_{0Bn=1}$ (sample No. 1)	2.5677 eV
$\omega_{0Bn=1}$ (sample No. 2)	2.56735 eV
$\omega_{LTBn=1}$	1.4 meV
ϵ_0	7.4

for sample Nos. 1 and 2. Therefore, we assume a damping spectrum $\Gamma(\omega)$ to be an unknown function of the photon energy $\hbar\omega$. In order to determine this function the following iteration procedure is performed. For each photon energy the damping is varied up to the greatest agreement between the measured and theoretical transmission due to Eqs. (1) and (2). The received damping spectrum $\Gamma(\omega)$ is plotted in Fig. 5 for different sample temperatures. In the low-frequency part $\omega < \omega_L$, the damping function of the lower polariton branch (LBP) is almost independent of temperature. This indicates collisions with impurities or point defects, as described earlier.[5] In the high-frequency part $\omega > \omega_L$, the damping $\Gamma(\omega)$ of the upper polariton branch (UBP) increases strongly with increasing temperature and with increasing detuning from the resonance frequency $\omega_{0An=1}$. Such a temperature dependence indicates a scattering of excitons by phonons.

In Fig. 6 we have plotted the temperature dependence of the UPB damping $\Gamma(\omega, T)$ for several photon energies $\hbar\omega$ between the $A_{n=1}$ and $B_{n=1}$ resonances. For a fixed photon energy and for $T > 10$ K the damping $\Gamma(T)$ is a straight line intersecting with the ordinate. The common intersection point Γ_{im} for different photon energies $\hbar\omega$ is due to impurity scattering, which, in our case, is different for sample Nos. 1 and 2. Furthermore, the gradient at a spectral position is equal for both samples. For high temperatures ($T > 10$ K) all curves can be fitted by a simple law in an isotropic and homogeneous medium, assuming a temperature-independent extrinsic term Γ_{im} due to impurity scattering and an intrinsic term $\Gamma_{ph}(\omega, T)$ due to acoustic-phonon scattering[1]

$$\Gamma(\omega, T) = \Gamma_{im} + \Gamma(\omega)^{T=0\,K} \frac{3K_B T}{2\hbar\omega_{ph}} \quad ; \quad T > 10\text{ K} , \quad (3)$$

where K_B is the Boltzmann constant and $\hbar\omega_{ph}$ the energy of the scattered phonon.

The scattering process of excitonic polaritons with acoustic phonons is sketched in Fig. 7. In the spectral range above the longitudinal exciton $\hbar\omega_L < \hbar\omega$, two propagation modes exist: the excitonlike LBP and the pho-
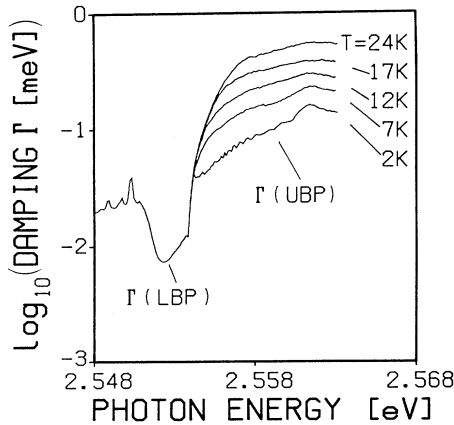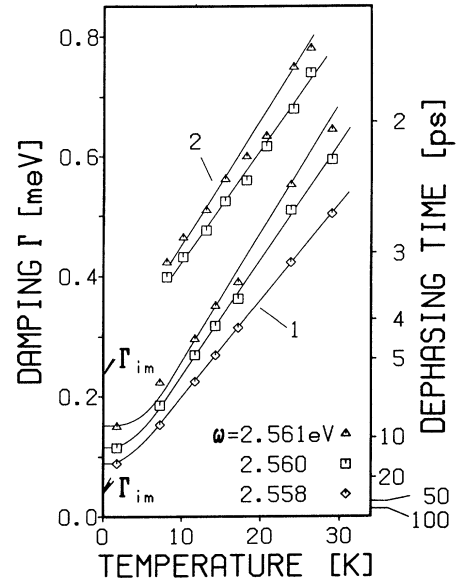

FIG. 6. Temperature dependence of the damping $\Gamma(T)$ for different photon energies showing linear dependences between Γ and T. Solid curves for $T < 10$ K are only to guide the eye. The intersection with the ordinate $\Gamma_{im} = 3.5 \times 10^{-5}$ eV and $\Gamma_{im} = 2.5 \times 10^{-4}$ eV for sample Nos. 1 and 2, respectively, are due to impurity scattering.

tonlike UBP. When an optical experiment in the range of the UBP is performed, the measured absorption is due to the emission or absorption of acoustic phonons. The scattering process has to satisfy the conservation rules of energy and momentum. Acoustic phonons have low energy and high momentum, so that photonlike polaritons are converted into excitonlike polaritons.

With Eq. (3) the energy of the phonon $\hbar\omega_{ph}$ involved in the scattering process can be estimated from the experimental damping spectra at $T = 2$ K and $T > 10$ K, assuming a homogeneous and isotropic medium. For

FIG. 5. Damping spectra $\Gamma(\omega)$ determined from transmission spectra measured at different temperatures for sample No. 1.
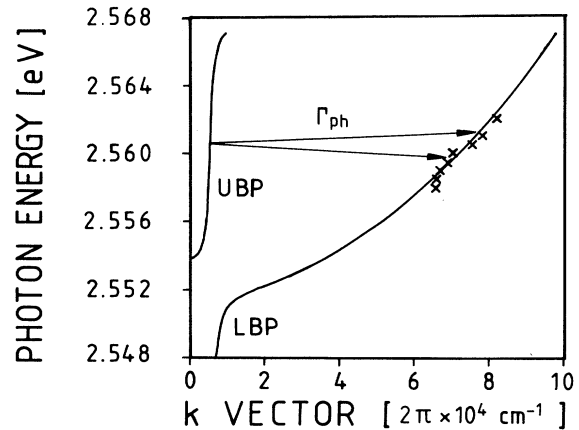

FIG. 7. Real part of the dielectric function of the exciton polariton calculated with the parameters from Table I and an averaged mass of $M = 0.95m_0$. The points are the final states of the scattering process estimated from the experiment (see text).

$\hbar\omega = 2.558$ eV we obtain $\hbar\omega_{ph} = 0.7$ meV, a value which is in accord to the value determined by Brillouin scattering experiments.[19] The estimated phonon energies $\hbar\omega_{ph}$ increase with increasing detuning from the resonance frequency $\omega_{0An=1}$, as expected for the scattering of polaritons from the UB to the LB by acoustic phonons. Neglecting the small transfer of phonon energy, the polariton wave vector of the final state in the scattering process k_{LBP} can be approximated by $k_{LBP} \approx |k_{UBP} - k_{LBP}| \approx \hbar\omega_{ph}/u_s$, where u_s is the sound velocity of TA phonons. The estimated k vectors of the polariton final states in the scattering process in Fig. 7 are fitted by the wave vectors calculated from the values in Table I and an average mass of $M = 0.95m_0$ has been chosen as a variable parameter. Based on the assumption of a homogeneous and isotropic medium we obtain an average mass $M = (M_\perp^2 M_\parallel)^{1/3}$ larger than the perpendicular mass $M_\perp = 0.9m_0$ and smaller than the parallel mass $M_\parallel = 2.7m_0$,[18] as expected for the scattering of polaritons by acoustic phonons in a solid angle 4π. Within the rough approximation of only one scattering channel, this clearly proves that absorption and emission of acoustic phonons dominates the measured absorption of exciton polaritons in this spectral region.

The increase in the gradient of the straight lines with increasing photon energy $\hbar\omega$ for $T > 10$ K in Fig. 6 results from the increase of $\Gamma(\omega)^{T=0\,K}$ with increasing detuning from the resonance frequency, which is partly compensated by the increase of $\hbar\omega_{ph}$, as discussed above, in the denominator of Eq. (3). In the next section we give a detailed analysis of the spectral shape $\Gamma(\omega)^{T=0\,K}$ to discriminate the different processes contributing to the scattering of polaritons by acoustic phonons.

IV. THE SCATTERING OF EXCITONIC POLARITONS WITH ACOUSTIC PHONONS

To determine the wave-vector dependence of the damping dispersion $\Gamma(k)$, the matrix elements of an exciton polariton transition from an initial state to a final state have to be calculated, whereby the scattering process with acoustic phonons has to satisfy the conservation rules of energy and momentum.[20,21] The transition is governed by the exciton content in the polariton mode, which is a slowly varying and negligible function approximating to unity around the exciton resonance.[22] Integration over all final states yields the result for the exciton-phonon interaction under consideration. Excitons can be scattered via the deformation potential (DP) and piezoelectric potential (PE) by acoustic phonons and via the Fröhlich potential by optical phonons.[20] The scattering by optical phonons gives no significant contribution for $T < 30$ K (Ref. 22) and will not be discussed here.

For the deformation-potential interaction the number of collisions per unit time of an upper branch polariton with a phonon system at 0 K is given by[1]

$$W(k)_{DP} = \frac{k^3}{2\pi\hbar v_g \rho u_s}(E_c - E_v)^2; \quad T = 0 \text{ K} \qquad (4)$$

where E_c and E_v are the deformation potentials of the

valence and conduction bands, u_s is the sound velocity, ρ is the crystal density and v_g and k the group velocity and wave vector of the polariton in its final state, respectively. In Eq. (4) the longitudinal-acoustic (LA) sound velocity has to be introduced. Transverse-acoustic (TA) waves can be neglected, because shear waves yield a very small deformation potential.

In hexagonal-type crystals such as CdS, exciton polaritons are further mediated by the piezoelectric effect. For this interaction the number of collisions per unit time of an upper branch polariton with a phonon system at 0 K is given by

$$W(k)_{PE} = \frac{k^5}{2\pi\hbar v_g \rho u_s}\left[a_B^2 \frac{2\pi e e_{av}}{\epsilon_0} \frac{m_e - m_h}{m_e + m_h}\right]^2; \quad T = 0 \text{ K}$$

$$\alpha_B = \frac{\hbar^2 \epsilon_0}{\mu^* e^2}; \quad \mu^* = \frac{m_e m_h}{m_e + m_h} \qquad (4')$$

where α_B is the exciton Bohr radius, e_{av} is the spherical average of the piezoelectric constants for the TA (LA) phonons calculated after the equations derived from Hutson,[23] e is the electron charge, and m_e, m_h are the electron and hole masses, respectively. For the derivation of Eqs. (4) and (4'), an isotropic and homogeneous medium has been assumed and the exciton masses are averaged in an ellipsoidal band. The corresponding equations for scattering of lower branch polaritons differ only by a prefactor and show the same wave-vector dependences as Eqs. (4) and (4'): $W_{UBP}(k) = \frac{3}{4}W_{LBP}(k)$.[24] For simplicity, we apply Eqs. (4) and (4') as well for the spectral region of the LBP below the longitudinal frequency, where the experimental absorption is nearly independent of temperature.

The collision terms Eqs. (4) and (4') have different wave vector and spectral dependences for the deformation-potential and piezoelectric potential interaction. Substituting $v_g = \hbar k/M$ in the spectral range $\omega > \omega_L$ we obtain for the scattering probability for the deformation interaction, $W(k)_{DP} \propto k^2 \propto \omega - \omega_0$, and for the piezoelectric interaction, $W(k)_{PE} \propto k^4 \propto (\omega - \omega_0)^2$. Calculations with the data for CdS yield that deformation-potential scattering Γ_{DP} dominates around and below the longitudinal frequency ω_L, while piezoelectric scattering Γ_{PE} becomes more and more dominant with increasing detuning from the lowest free exciton resonance.

From Eqs. (4) and (4'), we finally obtain for the damping dispersion $\Gamma(k)$ of exciton polaritons due to acoustic-phonon scattering

$$\Gamma(k)_{ph} = 2W(k)_{ph}$$
$$= 2[W(k)_{DP}^{LA} + W(k)_{PE}^{LA} + W(k)_{PE}^{TA}]; \quad T = 0 \text{ K}.$$

$$(5)$$

From the calculated damping dispersion $\Gamma(k)$ in Fig. 8, which is plotted as a function of photon energy $\hbar\omega$, it can be seen that the interaction of exciton polaritons with acoustic phonons vanishes below the exciton resonance frequency as observed in the experiment. On the low-energy wing of the $A_{n=1^-}$ exciton the experimental
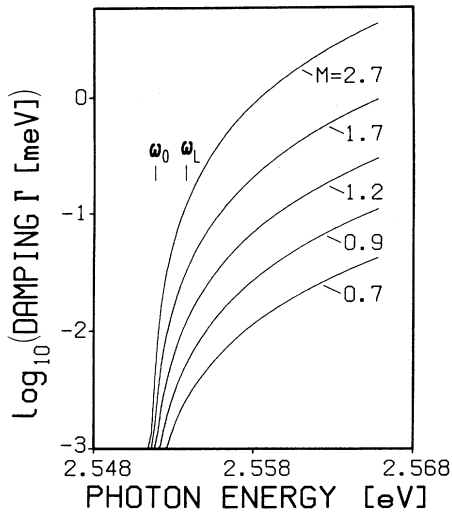
FIG. 8. Calculated damping dispersion of excitonic polaritons $\Gamma(\omega)$ due to acoustic-phonon scattering for different averaged exciton masses and $T=0$ K. For parameters see Tables I and II.

TABLE II. Parameter of the damping dispersion $\Gamma(k)$.

m_e	$0.2m_0$[a]
m_h	$0.7(k\perp c)$,[b] $1.6(k\|c)m_0$[c]
$E_c - E_v$	3.0 eV[d]
u_{TA}	$1.85(k\perp c)$, $1.76(k\|c)10^3$ m s^{-1}[e]
u_{LA}	$4.25(k\perp c)$, $4.50(k\|c)10^3$ m s^{-1}[e]
e_{31}	-0.244 C m^{-2}[f]
e_{33}	$+0.440$ C m^{-2}[f]
e_{15}	-0.210 C m^{-2}[f]

[a]Reference 18.
[b]From reflectance.
[c]Received from fit.
[d]Averaged value from Ref. 25.
[e]Reference 26.
[f]Reference 27.

transmission is purely extrinsic for low temperatures. The curves in Fig. 8 are determined from wave vectors received by Eq. (1) and with the parameters from Tables I and II. The calculated damping dispersions for different averaged exciton masses $M = (M_\perp^2 M_\|)^{1/3}$ reveal a strong increase of the scattering probability with increasing masses due to the wave-vector dependences in Eqs. (4) and (4').

To fit the measured damping spectrum (solid curve) at $T=2$ K in Fig. 9 we added to Eq. (5) an extrinsic damping term $\Gamma_{im}=2\times10^{-5}$ eV due to impurity scattering, which is about half the value obtained from the intersection with the ordinate in Fig. 6. For an average mass of $M=1.13m_0$ we obtain good agreement between experiment and theory in the spectral range outside the reso-
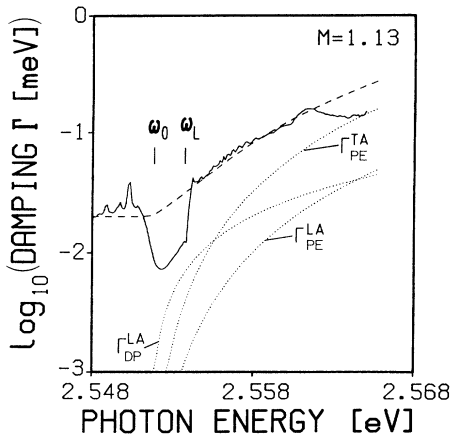
nance (dashed curve). In the region $\omega_0<\omega<\omega_L$ the damping spectrum is proportional to the polariton group velocity, and no description with this approach is possible.[5] Taking a perpendicular mass of $M_\perp=0.9m_0$ we determine a parallel mass of $M_\|=1.8m_0$ from the fit, which is slightly smaller than values known from the literature.[25]

Additionally, we have plotted in Fig. 9 the terms contributing to the intrinsic scattering by acoustic phonons due to Eqs. (4) and (4') via the deformation and piezoelectric potentials (dotted curves). Similar results can be received for sample No. 2 with the only difference of a much larger contribution of impurity scattering.

The only fitting parameter we have used in the description of the measured damping spectrum is the averaged exciton mass M and a term due to impurity scattering Γ_{im}. For the first the received value is close to the value given in the literature, and for the latter we got a similar value from the intersection with the ordinate in Fig. 6. All other numbers are taken from the analysis of reflectance spectra, or are known from the literature. We believe that our analysis of the damping dispersion is very convincing and clearly demonstrates that acoustic phonons and impurities contribute via different scattering processes to the measured damping spectrum above the free $A_{n=1}$ exciton resonance.

FIG. 9. Line-shape fit (dashed curve) of the measured damping spectrum $\Gamma(\omega)$ (solid curve). An extrinsic term $\Gamma_{im}=2\times10^{-5}$ eV due to impurity scattering is added to the intrinsic contributions due to phonon scattering (dotted lines) via the piezoelectric Γ_{PE} and deformation-potential interactions Γ_{DP} for TA (LA) transversal (longitudinal) acoustic phonons. For parameters see Tables I and II.

V. CONCLUSION

From precise measurement of reflectance and transmission we quantitatively determined the damping dispersion and discriminated different relaxation channels of exciton polaritons such as impurities and phonons. Above the free exciton resonance, upper branch polaritons are mainly converted by absorption or emission of acoustic phonons into lower branch polaritons. The calculated scattering probabilities for the deformation-potential interaction and the piezoelectric interaction agree well with the experimental results. In our investigations we chose CdS as a model material. However, our results can be applied to any spatial dispersive medium showing a piezoelectric effect.

[1]W. C. Tait and R. L. Weiher, Phys. Rev. 166, 769 (1968).

[2]P. Y. Yu and Y. R. Shen, Phys. Rev. B 12, 1377 (1975).

[3]R. G. Ulbrich and C. Weisbuch, in Festkörperprobleme XVIII: Advances in Solid State Physics, edited by J. Treusch (Vieweg, Braunschweig, 1978), Vol. 18, p. 217.

[4]T. Shigenari, X. Z. Lu, and H. Z. Cummins, Phys. Rev. B 30, 1962 (1984).

[5]I. Broser, K.-H. Pantke, and M. Rosenzweig, Phys. Status Solidi B 132, K117 (1985).

[6]M. Dagenais and W. F. Sharfin, Phys. Rev. Lett. 58, 1776 (1987).

[7]K.-H. Pantke and I. Broser, J. Lumin. 40&41, 499 (1988).

[8]K.-H. Pantke, Ph. D. thesis, Technische Universität Berlin, 1990.

[9]Y. Masumoto, S. Shionoya, and T. Takagahara, Phys. Rev. Lett. 51, 923 (1983).

[10]F. Vallée, F. Bogani, and C. Flytzanis, Phys. Rev. Lett. 66, 1509 (1991).

[11]K.-H. Pantke, P. Schillak, B. S. Razbirin, V. G. Lyssenko, and J. M. Hvam, Phys. Rev. Lett. 70, 327 (1993).

[12]C. E. Bleil, J. Phys. Chem. Solids 27, 1631 (1966).

[13]M. Azuma, J. Phys. Soc. Jpn. 22, 665 (1967).

[14]G. D. Mahan and J. J. Hopfield, Phys. Rev. 135, A428 (1964).

[15]E. S. Koteles, in Excitons, edited by E. I. Rashba and M. D. Sturge (North-Holland, Amsterdam, 1982), p. 83.

[16]S. I. Pekar, Zh. Eksp. Teor. Fiz. 34, 1176 (1958) [Sov. Phys. JETP 7, 813 (1958)].

[17]J. J. Hopfield and D. G. Thomas, Phys. Rev. 132, 563 (1963).

[18]M. Rosenzweig, Ph. D. thesis, Technische Universität Berlin, 1982.

[19]I. Broser and M. Rosenzweig, J. Phys. Soc. Jpn. A 49, 401 (1980).

[20]C. Weisbuch and R. G. Ulbrich, in Light Scattering in Solids III, edited by M. Cardona and G. Güntherodt (Springer-Verlag, Berlin, 1978), p. 207.

[21]M. Matsushita, J. Wicksted, and H. Z. Cummins, Phys. Rev. B 29, 3362 (1984).

[22]T. Takagahara, Phys. Rev. B 31, 8171 (1985).

[23]A. R. Hutson, J. Appl. Phys. 32, 2287 (1961).

[24]V. V. Travnikov and V. V. Krivolapchuk, Zh. Eksp. Teor. Fiz. 85, 2087 (1983) [Sov. Phys. JETP 58, 1210 (1983)].

[25]I. Broser, R. Broser, and M. Rosenzweig, in Physics of II-VI and I-VII Compounds, Semimagnetic Semiconductors, edited by O. Madelung, M. Schultz, and H. Weiss, Landolt-Börnstein New Series, Group III, Vol. 17, Pt. b (Springer-Verlag, Berlin, 1983), p. 166.

[26]D. Gerlich, J. Phys. Chem. Solids 28, 2575 (1967).

[27]D. Berlincourt, H. Jaffe, and L. R. Shiozava, Phys. Rev. 129, 1009 (1963).